BRNO UNIVERSITY OF TECHNOLOGY

Faculty of Electrical Engineering and Communication

Institute of Radio Electronics

Ing. Juraj Poliak

DIFFRACTION EFFECTS IN TRANSMITTED OPTICAL BEAM

SHORT VERSION OF PH.D. THESIS

Study field: Electronics and Communications
Supervisor: Prof. Ing. Otakar WILFERT, CSc.

DISERTACNÍ PRÁCE JE ULOŽENA:

Ústav radioelektroniky
Fakulta elektrotechniky a komunikačních technologií
Vysoké učení technické v Brně
Technická 12
616 00 Brno

CONTENTS

INTRODUCTION

> "If you would be a real seeker after truth, it is necessary that at least once in your life you doubt, as far as possible, all things." – René Descartes

Wireless optical signal transmission has many applications in communications nowadays – point-to-point connection (buildings, satellites), indoor communications inside buildings or public transport (Li-Fi as an alternative to Wi-Fi [1]) up to experimental applications (UV non-line-of-sight (NLOS) communications). The main advantage of using optical links, in comparison with RF (radio frequency) technology [2], is their non-licensed operation, significantly greater usable bandwidth, immunity against other EM sources [3] and last, but not least, high power efficiency and low weight, which makes them optimal for using in mobile and satellite communications.

Free-space optical (FSO, or optical wireless communication – OWC) links, which are of the main interest of the thesis, exploit the atmosphere as the transmission environment. In comparison with RF or MMW (milimetre wave) technology, the FSO links achieve much larger antenna gain and therefore it is possible to use beam with a very low divergence, which is in practice only a few milirads (terrestrial FSO links) down to a fraction of milirads (satellite communications)[4].

However, these advantages are often deteriorated by effects which give rise to some phenomena. FSO links performance is highly sensitive to outside atmospheric conditions. Another issue is also so far relatively low level of practical and theoretical experience with wireless optical links which have been studied mainly for last 30 years (whereas RF communications have already more than a century of development). This is linked with an insufficient or even a lack of a thorough analysis of many optical wave or geometrical effects, which are common in OWC systems. This often leads to omission of such effects during the phase of FSO link design. This is mainly caused by the fact that the main focus was so far to understand the optical properties of atmosphere and its influence on the optical wave. The shift of the focus of interest towards more advanced optical effects in OWC systems is mainly due to recent development in the photonics (more powerful optical sources), communication techniques (sophisticated modulations and codings) and optics (more advanced optical parts). This shift is also reflected in the thesis and is summarised by effects which are random, often omitted and non-standard.

1 STATE OF THE ART

1.1 Optical wireless communications

Free-space optical (FSO) links are used for optical signal transmission between a transmitter TX and a receiver RX in the atmospheric transmission media, mostly in troposphere. The optical beam between two FSO terminals propagates, in general, in a non-stationary and inhomogeneous atmospheric media. Maintaining the line-of-sight (LOS) between the terminals signal propagates over several hundreds of metres for terrestrial FSO links, up to thousands of kilometres for satellite links or deep-space links [5]. In order to maintain a stable, reliable link connection with high availability, optimisation in terms of the deterministic parameters of the transceiver with respect to the statistical parameters of the link location are needed.

FSO links are evaluated according to their availability and reliability. Availability is mostly influenced by the instantaneous state of the atmosphere [6] causing extinction, turbulent effects due to refractive index fluctuation in the atmosphere and by noise in general (background noise, thermal noise etc.). Lately, term "non-standard" effects began to be discussed. These effects cover not only atmospheric, but also wave and geometrical effects which are often hard to define quantitatively and which cause either the beam shape distortion or deteriorate the optical power measurements in testing FSO links.

1.2 Atmospheric effects in FSO systems

In FSO links in general, there is a technology shift in last years with the transceivers being equipped with optical fibre technology, which gives rise to fully photonic FSO links discussed also later in the thesis. In photonic links, optical fibre is used as the primary optical source in the transmitter. On the other hand, in the receiver, the optical beam is coupled directly to the optical fibre. This allows for much higher flexibility in the system design at the cost of much higher complexity. The crucial point is the optical beam reception from free-space with a receiving aperture diameter of several centimetres (or tens of centimetres) to the optical fibre core of several microns. High optical gain to be achieved causes a relatively narrow field of view (FOV), which gives rise to pointing errors. Lately, several design possibilities have been tested and presented worldwide. While Parca et al. [7] used a relatively simple approach combining a plano-convex lens and a GRIN-pigtailed fibre, Boroson et. al in [8] describe the Lunar Lasercom Space Terminal (LLST), where Cassegrain-Schmidt optical system have been used. While the first mentioned system is considered to be unreliable over larger distances in turbulent environment,

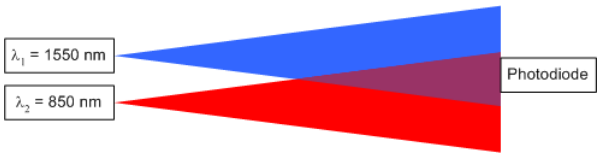

Fig. 1.1: Schematic of dual-wavelength FSO system

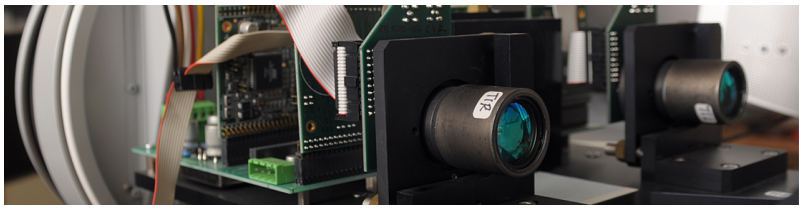

Fig. 1.2: Realisation of the dual-wavelength testing FSO transmitter at the Department of Radio Electronics, Brno University of Technology.

the latter is optimal, but would require investments too high for practical implementation in terrestrial FSO systems. Therefore, one of the goals of the dissertation has been set to analyse and to optimise FSO terminal design with respect to its optical and optomechanical structure, reliability and cost.

Testing FSO links serve to study spectral dependency of the atmospheric conditions on the optical beam attenuation and scintillation. For this purpose, so called dual testing FSO links have been developed [9] consisting of two separate terminals operating at different wavelengths (commonly 850 nm and 1550 nm). The current dual testing FSO link design is extremely sensitive to misalignments and a small thermal variation induces additional attenuation which might be misinterpreted as the impact of the measured atmospheric condition in the affected testing channel. This may lead to false conclusion that the operating wavelength is unsuitable for use in OWC.

There are some restrictions when two individual transmitters are used in case of transversally inhomogeneous fog event. Then, each of the optical beams is influenced in a different amount which leads again to misinterpretation of the measured data. Therefore, a thorough redesign of testing dual FSO links should be considered to merge both optical channels into a single optical channel. As will be shown in the thesis, this part is challenging not only practically but also theoretically.

1.3 Deterministic effects in FSO systems

This chapter deals with special (non-standard) effects, which are, however, not uncommon in FSO links. They have been called non-standard effects since their oc-

currence is highly random causing mainly attenuation and fluctuation of optical power and there is lack of thorough mathematical analysis of such effects. Many teams worldwide work on their identification and description (COST Action IC1101: http://opticwise.uop.gr/), which is a complex task since they rarely occur separately from other effects.

1.3.1 Geometrical loss

Common practice is to estimate the misalignment error of FSO link (usually 1 – 3 dB). Taking into account the beam divergence, one may find the geometrical loss for circularly symmetrical beam [10]. Literature survey points out the lack of an exact model describing precisely the case of an elliptically symmetrical Gaussian beam which is generated by common semiconductor laser diodes (LD).

A solution actively sensing misalignments is to use an automatic pointing, acquisition and tracking (PAT) system. Using a beacon, the PAT system points the terminal towards a receiver with larger FOV than the communication link. This is carried out for both directions and after succesful acquisition, the PAT system tracks small changes in terminal direction to maintain line-of-sight (LOS) a increase the system availability. System allows to decrease the divergence angle FOV to increase the range of such system or in mobile communications. Higher costs make such system mostly used for satellite communications.

To evaluate the system sensitivity to atmospheric and geometrical effects, one uses the FSO link budget. The result of the link budget analysis is the link margin M [4]. Its value defines the acceptable attenuation caused by atmospheric effects, misalignments, aging or mechanical instability to achieve required FSO link reliability and availability. The percentage of time over a period when the link margin is larger than zero defines the link availability, which is a key design parameter and is given by the particular link application and nature of the transmitted signal.

Analysis of all individual effects gives rise to a complex model of optical wireless communications which quantifies with a given precision individual effects.

1.3.2 Diffraction effects

As is shown in Fig.1.3, the Fresnel diffraction pattern of an optical wave observed behind a circular aperture shows no longer a smooth exponential decline of the optical intensity from the beam centre towards its edges, but rather complicated structure with a number of maxima and minima. In the worst-case scenario, we might have the diameter of the central maximum larger than the diameter of the receiver aperture RXA. Then, when ideally aligned, the received optical power is

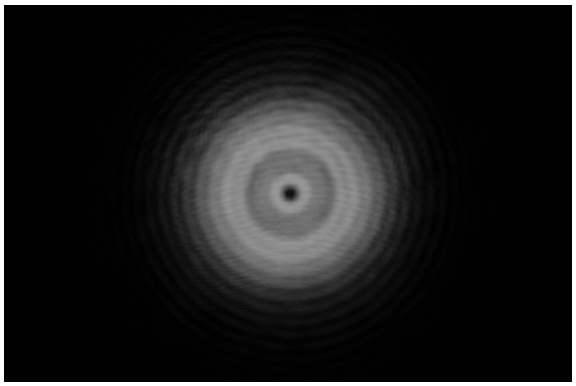

Fig. 1.3: Experimental observation of the Fresnel diffraction in the planar optical beam transmission. Wavalength $\lambda = 632.8$ nm, TXA radius $r_{\mathrm{TXA}} = 4.0$ mm, beam radius in the TXA plane $w_{\mathrm{TXA}} = 14$ mm, distance $L = 6.32$ mm, which corresponds to the number N_{f} of observable Fresnel zones at the distance L $N_{\mathrm{f}} = 4$.

zero. If, however, one aligns the FSO link in the direction of the first maximum, the atmospheric scintillation increases the variance of the received power. This is mainly due to very sharp and narrow distribution of the optical intensity at the first maximum. The thesis presents how to analyse the problem of Fresnel diffraction, quantitatively assess its influence on the particular FSO link performance and how to minimise its effects to a reasonable level.

2 OBJECTIVES OF THE THESIS

Based on the actual state-of-the-art in the field of OWC, following thesis objectives have been proposed:

- Develop analytical model of the diffraction of an elliptically symmetrical generally astigmatic Gaussian beam on a circularly symmetrical transmitter aperture
- Develop analytical model of the geometrical attenuation of an elliptical Gaussian beam restricted by a circular optical system
- Develop analytical model of the attenuation due to misalignment of an elliptical Gaussian beam
- Based on the synthesis of the preceding objectives, propose methods and terminal design improvements to increase reliability and availability of both testing and data FSO links

3 WAVE EFFECTS IN OWC

The optical radiation is an electromagnetic (EM) radiation covering ultraviolet (UV), visible (VIS) as well as infrared (IR) part of the spectra. The optics is part of the physics, which analyses properties of the optical radiation and its interaction with the matter, can be divided into four disciplines with increasing complexity; geometrical, electromagnetic, wave and quantum optics.

3.1 Gaussian beam

An expression of the wave function ψ of the Gaussian beam with elliptically symmetrical distribution is given by

$$\begin{aligned}\psi\left(x,y,z\right) &= \sqrt{\tfrac{w_{0x}w_{0y}}{w_x w_y}}\exp\left[-\left(\tfrac{x}{w_x}\right)^2-\left(\tfrac{y}{w_y}\right)^2\right]\cdot \\ \cdot\exp&\left\{\mathrm{i}k\left[z+\tfrac{x^2}{2R_x}+\tfrac{y^2}{2R_y}+\arctan\left(\tfrac{k\left(w_{0x}^2+w_{0y}^2\right)}{2z-kw_{0x}w_{0y}}\right)\right]+\mathrm{i}\tfrac{\pi}{2}\right\},\end{aligned} \tag{3.1}$$

where w_{0x} and w_{0y} are beam half-widths in beam waist in x and y axis, respectively and w and R are beam half-widths and beam radii in x and y axis, respectively [11]. The detected optical intensity distribution $I(x,y,z)$ of an elliptically symmetrical planar Gaussian beam is

$$I\left(x,y,z\right)=\frac{w_{0x}w_{0y}}{w_x w_y}\exp\left[-2\left(\frac{x^2}{w_x^2}+\frac{y^2}{w_y^2}\right)\right]. \tag{3.2}$$

3.2 Fresnel diffraction integral

Diffraction integral for Fresnel diffraction effects can be derived by substituting spherical wave ψ_0 by its Fresnel approximation

$$\psi\left(P\right)=-\frac{\mathrm{i}}{\lambda}\iint_{\Sigma_{\mathrm{TXA}}}\psi_0\left(x_{\mathrm{M}},y_{\mathrm{M}}\right)\exp\left\{\frac{\mathrm{i}k}{2z}\left[\left(x-x_{\mathrm{M}}\right)^2+\left(y-y_{\mathrm{M}}\right)^2\right]\right\}\,\mathrm{d}x_{\mathrm{M}}\,\mathrm{d}y_{\mathrm{M}}. \tag{3.3}$$

Subsequently, by expanding the square in the phasor and small modification one comes to the Fresnel diffraction integral

$$\begin{aligned}\psi(x,y,z)=-\frac{\mathrm{i}}{\lambda}\frac{\exp\left(\mathrm{i}kz\right)}{z}\exp\left[\frac{\mathrm{i}k}{2z}\left(x^2+y^2\right)\right]\iint_{\Sigma_{\mathrm{TXA}}}\psi_0\left(x_{\mathrm{M}},y_{\mathrm{M}}\right)\times \\ \times\exp\left[\frac{\mathrm{i}k}{2z}\left(x_{\mathrm{M}}^2+y_{\mathrm{M}}^2\right)\right]\exp\left[-\frac{\mathrm{i}k}{z}\left(xx_{\mathrm{M}}+yy_{\mathrm{M}}\right)\right]\,\mathrm{d}x_{\mathrm{M}}\,\mathrm{d}y_{\mathrm{M}},\end{aligned} \tag{3.4}$$

where the wave function characterising Fresnel diffraction integral is expressed in form of Fourier transform of product of the wave function ψ_0 at the plane of diffraction aperture (in OWC TX lens socket) and of the phasor $\exp\left[\frac{ik}{2z}\left(x_{\mathrm{M}}^2 + y_{\mathrm{M}}^2\right)\right]$. Fraunhofer diffraction phenomena may be regarded as a special case of more general Fresnel diffraction when this phasor is one (i.e. when the $z \to \infty$), or more precisely, when it oscillates slow enough to be taken out of the integral in (3.4). To distinguish between various diffraction scenarios, one may effectively calculate the number of the Fresnel zones observed in the observation plane Σ_{RXA} represented by the Fresnel number N_{f}.

Fraunhofer region (also called far-field zone) is the region where $N_{\mathrm{f}} \ll 1$. As the N_{f} approaches and exceeds one, the phasor discussed in Eq. (3.4) becomes relevant and resulting diffraction effects are called Fresnel diffraction. This region is often referred to as near-field zone. Not only in the optical instrumentation and in the laboratory is Fresnel diffraction limiting factor, but should also be taken into account during FSO link design. For instance, when one-inch transmitter optics (r_{TXA}) and wavelength $\lambda = 1550$ nm are considered, the near-field zone boundary (Rayleigh distance) is as far as $z = 416$ m. In many instances, the terrestrial FSO links do not exceed this distance and, therefore, work in the near-field zone.

An important part of the calculation is the right mathematical expression of the primary wave function ψ_0 into diffraction integral respecting the physical properties of the transmitted beam. In practice, one should always consider diffraction of an elliptically symmetrical spherical wave on a circularly symmetrical aperture, which, however, excludes almost any analytical calculation. Another important aspect to take into account is the curvature radius of the wavefront, which depends on the beam divergence angle and last, but not least, the beam astigmatism. These effects form the main research focus of author.

3.3 Fresnel diffraction in form of integration of Bessel functions

Following section provides derivation and description of the Fresnel diffraction integral in terms of Bessel function integration for circularly symmetrical scenario. Let the planar optical wave with constant intensity distribution illuminate a circular aperture of the radius ρ_0 in an opaque screen. The distance s between M and P can be in cylindrical coordinates expressed in terms of Fresnel approximation as [12]

$$s^2 = \rho^2 + r^2 - 2\rho r \cos\left(\varphi - \theta\right) + z^2, \tag{3.5}$$

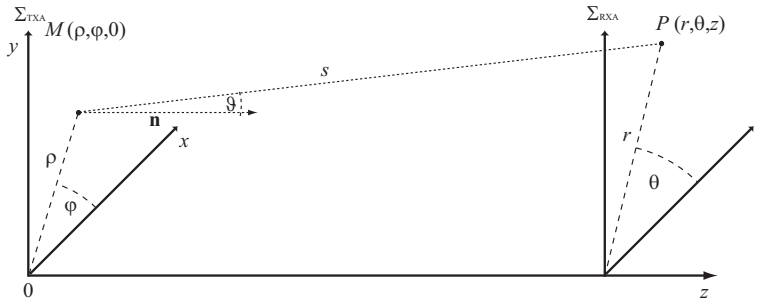

Fig. 3.1: To the explanation of Hyugens-Fresnel principle in cylindrical coordinates.

which yields

$$\frac{\exp\left(\mathrm{i}ks\right)}{s} \approx \frac{\exp\left[\mathrm{i}k\left(z+\frac{r^2}{2z}\right)\right]}{z} \exp\left\{\frac{\mathrm{i}k}{2z}\left[\rho^2 - 2\rho r\cos\left(\varphi-\theta\right)\right]\right\}. \tag{3.6}$$

Taylor expansion used for the approximation limits the validity of the expression and defines the validity condition defined as

$$z > \frac{r_{\mathrm{TXA}}^2 \pi}{2\lambda}. \tag{3.7}$$

Now, the wave function at the observation point P in the receiver plane Σ_{RXA} is

$$\psi\left(P\right) = -\frac{\mathrm{i}}{\lambda}\frac{\exp\left[\mathrm{i}k\left(z+\frac{r^2}{2z}\right)\right]}{z}\int_0^{r_{\mathrm{TXA}}}\exp\left(\frac{\mathrm{i}k}{2z}\rho^2\right)\int_0^{2\pi}\exp\left[-\frac{\mathrm{i}k}{z}\rho r\cos\left(\varphi-\theta\right)\right]\mathrm{d}\varphi\rho\mathrm{d}\rho, \tag{3.8}$$

where the exponential term in the inner integral may be solved using expression (3.915-2.) in [13]. Then the observed wave function takes form

$$\psi\left(\rho, N_{\mathrm{f}}\right) = -2\pi\mathrm{i}N_{\mathrm{f}}\exp\left[\mathrm{i}\left(\frac{2\pi}{\lambda}z+\pi N_{\mathrm{f}}\rho^2\right)\right]\int_0^1\exp\left(\pi\mathrm{i}N_f t^2\right)J_0\left(2\pi N_{\mathrm{f}}\rho t\right)t\mathrm{d}t. \tag{3.9}$$

Finally, using the Euler's formula (to avoid dealing with complex exponential functions), the intensity at the observation point P is given by

$$\begin{aligned} I(\rho, N_{\mathrm{f}}) = |\psi\psi*|^2 = \left(2\pi N_{\mathrm{f}}\right)^2 \Bigg\{ \Bigg[\int_0^1 \cos\left(\pi N_f t^2\right) J_0\left(2\pi N_{\mathrm{f}}\rho t\right) t\mathrm{d}t\Bigg]^2 + \\ + \Bigg[\int_0^1 \sin\left(\pi N_{\mathrm{f}} t^2\right) J_0\left(2\pi N_{\mathrm{f}}\rho t\right) t\mathrm{d}t\Bigg]^2 \Bigg\}. \end{aligned} \tag{3.10}$$

As was already mentioned, there are only a few scenarios, where an exact analytical solution is possible. However, the expression in (3.10) is not the case. Therefore, a numerical solution must be carried out in order to calculate the integral in it and to evaluate the wave function at the observation point P.

3.4 Fresnel diffraction in form of FFT

Section 3.2 introduced the Fresnel diffraction integral defined in terms of the Fourier Transform in Cartesian coordinates, which can be used for more efficient computer processing of diffraction pattern simulation compared to solutions expressed in cylindrical coordinates. It benefits from numerical methods to speed up the calculation of Fourier Transform. These methods, however, require gentle treatment and full understanding of physical principles and effects that occur during diffraction [14]. Direct substitution of the Fresnel approximation of the wave into Eq. (3.4) and its modification yields wave function of the diffracted wave in the plane of observation Σ_{RXA}

$$\psi(x,y,z) = -\frac{\mathrm{i}}{\lambda}\frac{\exp\left[\mathrm{i}k\left(z'+z\right)\right]}{z'z}\exp\left[\frac{\mathrm{i}k}{2z}\left(x^2+y^2\right)\right]\cdot$$
$$\mathcal{F}\left\{\mathrm{circ}\left(\frac{x_{\mathrm{M}}^2+y_{\mathrm{M}}^2}{r_{\mathrm{TXA}}^2}\right)\exp\left\{x_{\mathrm{M}}^2\left[\frac{\mathrm{i}k}{2}\left(\frac{1}{z_1}+\frac{1}{z}\right)-\frac{1}{w_x^2}\right]+y_{\mathrm{M}}^2\left[\frac{\mathrm{i}k}{2}\left(\frac{1}{z_2}+\frac{1}{z}\right)-\frac{1}{w_y^2}\right]\right\}\right., \tag{3.11}$$

where $z' = \sqrt{z_1 z_2}$, $\mathcal{F}$ stands for the Fourier Transform.

The main objective of the simulation of Fresnel diffraction effects leads to the estimation of the minimal distance of the FSO link operation without any disturbance in the optical intensity distribution of the transmitted beam due to the beam restriction caused by the transmitter optics.

3.5 Diffraction effect assessment

3.5.1 Model based on the Bessel functions integration

The Bessel-based model in (3.10) shows in Fig.3.3a) how the circular Gaussian beam intensity distribution changes due to diffraction along the link path. In order to compare the model with precise, but a computationally demanding, calculation of the diffraction effects based on Rayleigh-Sommerfeld integral presented in [15] and also for more general comparison, axial distance along the link path is shown in the units of aperture radii. First, comparing Fig.3.3a) and Fig.3.3b) [15] one may see that the benefit of using a much simpler calculation did not influence the overall results which are objectively similar. Furthermore, it is clearly visible that as we move the receiver plane Σ_{RXA} along the optical axis, there are several positions on the z axis, where the optical intensity at the optical axis is zero and also areas where the contrast of the diffraction pattern is maximal. This is, for instance, visible at $z \approx 4.7 \cdot r_{\mathrm{TXA}}$, i.e. where $N_{\mathrm{f}} = 2$. More precisely, the beam intensity distribution

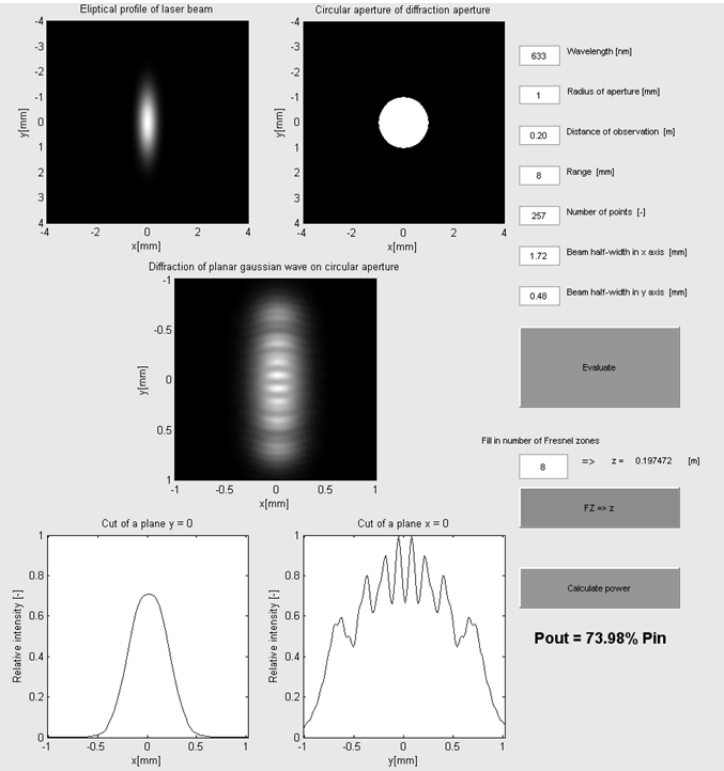

Fig. 3.2: Simulation of Fresnel diffraction effect in FSO systems. Top left - primary elliptical Gaussian beam with beam-widths $w_x = 1.72$ mm and $w_y = 0.48$ mm in x and y axis, respectively. Top right - circular aperture (TXA) with radius $r_{\mathrm{TXA}} = 1$ mm. Central plot shows the diffracted beam in the plane of observation r_{RXA} and bottom left and right - optical intensity of the diffracted beam along x and y axis, respectively. In the bottom left section, power P_{out} transmitted through the circular aperture is calculated relative to the total radiated power P_{in} of the optical source.

changes with changing number of observed Fresnel zones N_{f}, which changes with z, which gives rise also to relation between contrast C and Fresnel number N_{f}.

3.5.2 Model based on the FFT

Figure 3.2 shows the simulation of the FFT-based diffraction model. After filling the simulation parameters on the right-hand side of the window, the computer performs the FFT calculation in (3.4) to evaluate the diffraction of the elliptical optical wave (in the upper-left corner of the window) on a circular aperture (upper-right). The result in the receiver plane Σ_{RXA} is shown in the middle. Cross-sections through the center of the optical beam along the x and y axes are shown in the bottom-left and bottom-right corner, respectively.

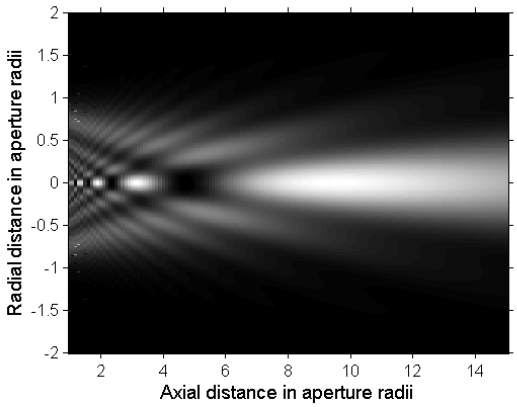

(a)

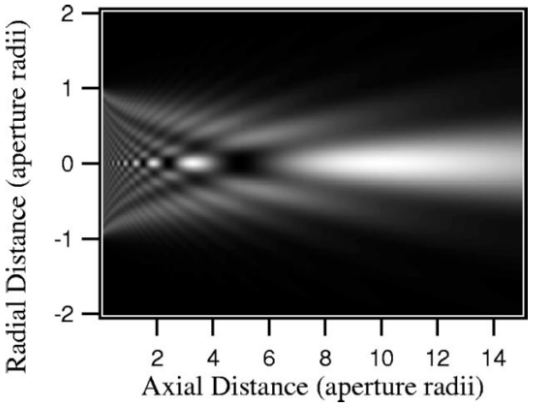

(b)

Fig. 3.3: a) Intensity distribution calculated using the method of integration of the Bessel functions as a function of both radial and axial distance from the aperture in the units of the aperture radius r_{TXA} according to (3.10).
b) Calculated intensity distributions using the complete Rayleigh-Sommerfeld model [15]. Simulation parameters: $\lambda = 10.6$ µm and $r_{\mathrm{TXA}} = 0.1$ mm. The boundary between near field and far field is located around $z \approx 9.4 \cdot r_{\mathrm{TXA}}$.

The situation in Fig.3.2 also shows the scenario when nearly eight Fresnel zones are observed, i.e. $N_{\mathrm{f}} \approx 8$. Since the ratio $\frac{w_y}{r_{\mathrm{TXA}}}$ is around one half, we can see the effect of the diffraction contrast reduction in the beam cross-section along the y axis, i.e. the diffraction effect is not observed.

The beam restriction gives rise not only to the diffraction effects. Another, not less significant aspect described in [16] is the power attenuation. The model presented in Fig.3.2 also shows in the bottom-left corner the portion of the power transmitted through the transmitter optical system and will be in detail described in Chapter 4.

4 GEOMETRICAL AND POINTING LOSS

When the FSO link is aligned ideally, the beam optical axis and aperture axis of symmetry are identical. Optical power attenuation on RXA, when no turbulence effects are taken into account, is defined by the relative size of the beam w_{RXA} and the radius r_{RXA} and is called geometrical loss α_{geom} (cf. Fig.4.1). Additional attenuation occurs when the beam and aperture axes are not identical, which gives rise to the misalignment loss α_{mis}, sometimes also referred to as pointing error. The degree of the misalignment is quantified by tilt angle γ_{t} (cf. Fig.4.3).

Optical power P of the beam is defined

$$P(z) = \iint_{-\infty}^{\infty} I(x, y, z)\mathrm{d}S, \tag{4.1}$$

where S is unrestricted part of the surface of the beam (theoretically infinite for unrestricted beam). In case of an elliptically symmetrical Gaussian beam described by Eq. (3.2), the total optical power P_0 is

$$P_0(z) = \iint_{-\infty}^{\infty} I\left(0, 0, z\right) \exp\left[-2\left(\frac{x^2}{w_x^2} + \frac{y^2}{w_y^2}\right)\right]\mathrm{d}S = I\left(0, 0, z\right)\frac{\pi}{2} w_x w_y, \tag{4.2}$$

where $I\left(0, 0, z\right)$ is the axial optical intensity of the beam at the distance z.

Geometrical attenuation is determined by the part of the optical power transmitted from TX, which is not received by an optical receiver RX with a finite aperture with radius r_{RXA} (or r_{TXA}) at the distance z mainly due to the beam divergence θ. However, it is more efficient to calculate the part P_{t} of the beam, which is received by the receiver aperture (RXA) and divide it by the total optical power P_0 (4.2) in order to estimate the losses. Now, four different calculations of a geometrical loss depending on the distance z and the radius of the receiver aperture r_{RXA} will be introduced - two exact formulas (4.8) and (4.12) requiring numerical integration and two approximative formulas (4.15) and (4.18). Following text shows the step-by-step derivation of these expressions.

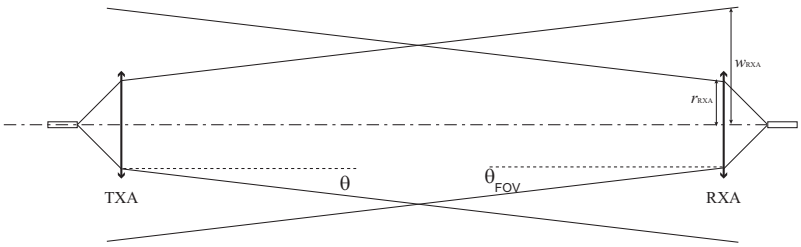

Fig. 4.1: To the explanation of geometrical attenuation loss.

4.1 Derivation of exact expressions

Power P_t of an elliptical beam with beam-widths w_x and w_y received by a circular aperture with radius r_RXA is given by

$$P_\mathrm{t} = I\left(0,0,z\right) \iint\limits_{x^2+y^2\leq r_\mathrm{RXA}} \exp\left[-2\left(\frac{x^2}{w_x^2}+\frac{y^2}{w_y^2}\right)\right]\mathrm{d}x\ \mathrm{d}y, \tag{4.3}$$

which in polar coordinates (ρ,φ) yields

$$P_\mathrm{t} = 4I\left(0,0,z\right) \int\limits_0^{r_\mathrm{RXA}} \int\limits_0^{\pi/2} \exp\left[-2\rho^2 \underbrace{\left(\frac{\cos^2\varphi}{w_x^2}+\frac{\sin^2\varphi}{w_y^2}\right)}_{A}\right]\mathrm{d}\varphi\rho\ \mathrm{d}\rho. \tag{4.4}$$

I. Integration first according to ρ

First, let's integrate Eq. (4.4) according to the radial variable ρ and substitute for $t = 2A\rho^2$, which yields

$$\int\limits_0^{r_\mathrm{RXA}} \exp\left(-2A\rho^2\right)\rho\ \mathrm{d}\rho = \frac{1}{4A}\int\limits_0^{2Ar_\mathrm{RXA}^2} \exp\left(-t\right)\ \mathrm{d}t = \frac{1}{4A}\left[1-\exp\left(-2Ar_\mathrm{RXA}^2\right)\right]. \tag{4.5}$$

Then, for the power P_t we may write

$$\begin{aligned} P_\mathrm{t} &= \int\limits_0^{\pi/2} \frac{I\left(0,0,z\right)}{A}\left[1-\exp\left(-2Ar_\mathrm{RXA}^2\right)\right]\mathrm{d}\varphi = \\ &= I\left(0,0,z\right)\underbrace{\int\limits_0^{\pi/2}\frac{\mathrm{d}\varphi}{A}}_{I_1} - I\left(0,0,z\right)\underbrace{\int\limits_0^{\pi/2}\frac{\exp\left(-2Ar_\mathrm{RXA}^2\right)}{A}\mathrm{d}\varphi}_{I_2}. \end{aligned} \tag{4.6}$$

However, the integral I_2, to the best of my knowledge, has no analytical solution. Therefore, one must solve I_2 by means of other methods, e.g. numerical integration. Now, the power P_t is from Eq. (4.6)

$$\begin{aligned} P_\mathrm{t} &= I\left(0,0,z\right)\left(I_1-I_2\right) = \\ &= I\left(0,0,z\right)\tfrac{\pi}{2}w_xw_y - I\left(0,0,z\right)\tfrac{w_x^2w_y^2}{w_x^2+w_y^2}\exp\left(-r_\mathrm{RXA}^2\tfrac{w_x^2+w_y^2}{w_x^2w_y^2}\right)I_3\left(r_\mathrm{RXA}^2\right) = \\ &= I\left(0,0,z\right)\frac{\pi}{2}w_xw_y\left[1-\frac{2}{\pi}\frac{w_xw_y}{w_x^2+w_y^2}\exp\left(-r_\mathrm{RXA}^2\frac{w_x^2+w_y^2}{w_x^2w_y^2}\right)I_3\left(r_\mathrm{RXA}^2\right)\right]. \end{aligned} \tag{4.7}$$

Note, that I_1 in the calculation represents the overall beam power and I_2 the part of the power, which is shadowed by the aperture leaving only the transmitted power P_t. In practical application, we rather than expressing optical power transmitted

through an optical system define the attenuation of the restricted part of the beam. First exact solution $\alpha_{\mathrm{ex},1}$ yields

$$\alpha_{\mathrm{ex},1} = \frac{P_{\mathrm{t}}}{P_0} = 1 - \frac{2}{\pi}\frac{w_x w_y}{w_x^2 + w_y^2}\exp\left(-r_{\mathrm{RXA}}^2 \frac{w_x^2 + w_y^2}{w_x^2 w_y^2}\right) \int_0^{\pi} \frac{\exp\left(\frac{w_x^2 - w_y^2}{w_x^2 w_y^2} r_{\mathrm{RXA}}^2 \cos\varphi\right)}{1 - \frac{w_x^2 - w_y^2}{w_x^2 + w_y^2}\cos\varphi} \mathrm{d}\varphi, \tag{4.8}$$

where $\alpha_{\mathrm{ex},1}$ stands for the (first) exact analytical expression of the geometrical attenuation of an elliptical Gaussian beam on a circular aperture, which can be used in the FSO link budget calculations. However, expression (4.8) can only be solved by means of numerical integration methods. Therefore, we now show the integration of integrals in Eq.(4.4) in a different order.

II. Integration first according to φ

Now, we first integrate integrals in Eq.(4.4) according to the angular variable.

The power P_t is

$$P_{\mathrm{t}} = 2\pi I\left(0,0,z\right) \int_0^{r_{\mathrm{RXA}}} \exp\left[-\rho^2\left(\frac{1}{w_x^2} + \frac{1}{w_y^2}\right)\right] I_0\left(\rho^2 \frac{w_x^2 - w_y^2}{w_x^2 w_y^2}\right) \rho \, \mathrm{d}\rho. \tag{4.9}$$

Substitution

$$t = \left(\frac{\rho}{r_{\mathrm{RXA}}}\right)^2 \tag{4.10}$$

yields for the power P_t

$$P_{\mathrm{t}} = \pi r_{\mathrm{RXA}}^2 I\left(0,0,z\right) \int_0^1 \exp\left(-r_{\mathrm{RXA}}^2 \frac{w_x^2 + w_y^2}{w_x^2 w_y^2} t\right) I_0\left(r_{\mathrm{RXA}}^2 \frac{w_x^2 - w_y^2}{w_x^2 w_y^2} t\right) \mathrm{d}t. \tag{4.11}$$

Again, the expression for power P_{t} has no analytical solution. For the second exact expression of geometrical attenuation $\alpha_{\mathrm{ex},2}$ we may now write

$$\alpha_{\mathrm{ex},2} = \frac{P_{\mathrm{t}}}{P_0} = \frac{2r_{\mathrm{RXA}}^2}{w_x w_y} \int_0^1 \exp\left(-r_{\mathrm{RXA}}^2 \frac{w_x^2 + w_y^2}{w_x^2 w_y^2} t\right) I_0\left(r_{\mathrm{RXA}}^2 \frac{w_x^2 - w_y^2}{w_x^2 w_y^2} t\right) \mathrm{d}t. \tag{4.12}$$

Despite the fact that both Eq.(4.8) and Eq.(4.12) have no analytical solution, they provide equivalent and valid results.

4.2 Derivation of approximative expressions

This section provides derivation of approximative analytical solution to exact geometrical loss expressions derived in the previous section. First, according to Equation (8.447-1) in [13] we can approximate the modified Bessel function I_0 as

$$I_0\left(z\right) = \sum_{k=0}^{\infty} \frac{\left(\frac{z}{2}\right)^{2k+1}}{\left(k!\right)^2} \approx 1 + \frac{z^2}{4} + \frac{z^4}{64} + \frac{z^6}{2304} = \left(1 + \frac{z}{2} + \frac{z^2}{8}\right)^2 + \frac{z^6}{2304}. \tag{4.13}$$

Before validity of the geometrical attenuation approximation based on Eq. (4.13) is further discussed, another approximation approach will be introduced. That is based on an asymptotic approximation of the modified Bessel function I_0 (for large values of $|z|$) by Eq. (8.451-5) in [13]

$$I_0(z) \approx \frac{\exp(z)}{\sqrt{2\pi z}}. \tag{4.14}$$

According to the definition, the approximation in Eq. (4.14) can be used for larger values of argument of modified Bessel function in Eq. (4.12), unlike the approximation in Eq. (4.13). The value of this function for $z = 0$ is infinity and is minimal for $z = 0.5$, where $I_0 = 0.93$. When $z > 1$, the approximated value is constantly smaller than the precise value and the difference does not exceed 2%, which is acceptable compared to the measurement error.

Therefore, one may conclude that when the argument if I_0 in Eq. (4.12) is $z \leq 1$, its approximation based on Eq. (4.13) containing first three terms can be used. For larger values of argument, one may use expression (4.14). Now, final approximative expressions of geometrical attenuation α_{app} are shown in the following text.

First, approximation of I_0 in (4.12) by (4.13) yields (first) approximative expression for geometrical attenuation $\alpha_{\text{app},1}$

$$\begin{aligned}\alpha_{\text{app},1} = \quad & \frac{2r_{\text{RXA}}^2}{w_x w_y}\Big[\int_0^1 \exp(-\alpha t)\ \mathrm{d}t + \\ & + \frac{\beta^2}{4}\int_0^1 t^2 \cdot \exp(-\alpha t)\ \mathrm{d}t + \\ & + \frac{\beta^4}{64}\int_0^1 t^4 \cdot \exp(-\alpha t)\ \mathrm{d}t\Big], \text{for } u \leq 1\end{aligned} \tag{4.15}$$

where

$$\alpha = r_{\text{RXA}}^2 \frac{w_x^2 + w_y^2}{w_x^2 w_y^2}, \tag{4.16a}$$

$$\beta = r_{\text{RXA}}^2 \frac{w_x^2 - w_y^2}{w_x^2 w_y^2}, \tag{4.16b}$$

$$u = r_{\text{RXA}}^2 \frac{w_x^2 - w_y^2}{w_x^2 w_y^2} t, \tag{4.16c}$$

$$t = \left(\frac{\rho}{r_{\text{RXA}}}\right)^2. \tag{4.16d}$$

Second approximative expression is obtained by means of approximation of I_0 in (4.12) by (4.14). This approach actually provides means of analytical solution. In order to effectively compute this integral, I recommend the backwards substitution

(4.10) in (4.12) prior to the approximation as follows

$$\begin{aligned}
\alpha_{\text{app},2} &= \frac{4}{w_x w_y} \int_0^{r_{\text{RXA}}} \exp\left(-\rho^2 \frac{w_x^2 + w_y^2}{w_x^2 w_y^2}\right) I_0\left(\rho^2 \frac{w_x^2 - w_y^2}{w_x^2 w_y^2}\right) \rho \mathrm{d}\rho = \\
&= \sqrt{\frac{8}{\pi\left(w_x^2 - w_y^2\right)}} \int_0^{r_{\text{RXA}}} \exp\left(-\rho^2 \frac{w_x^2 + w_y^2}{w_x^2 w_y^2}\right) \exp\left(\rho^2 \frac{w_x^2 - w_y^2}{w_x^2 w_y^2}\right) \mathrm{d}\rho = \\
&= \sqrt{\frac{8}{\pi\left(w_x^2 - w_y^2\right)}} \int_0^{r_{\text{RXA}}} \exp\left[\rho^2 \left(\frac{w_x^2 - w_y^2}{w_x^2 w_y^2} - \frac{w_x^2 + w_y^2}{w_x^2 w_y^2}\right)\right] \mathrm{d}\rho = \\
&= \sqrt{\frac{8}{\pi\left(w_x^2 - w_y^2\right)}} \int_0^{r_{\text{RXA}}} \exp\left[-\rho^2 \frac{2}{w_x^2}\right] \mathrm{d}\rho.
\end{aligned} \tag{4.17}$$

Modification using Eq.(3.321-2) in [13] yields the (second) approximative expression of geometrical attenuation

$$\alpha_{\text{app},2} = \frac{w_x}{\sqrt{w_x^2 - w_y^2}} \operatorname{erf}\left(\sqrt{2} \frac{r_{\text{RXA}}}{w_x}\right), \text{for } u > 1, \tag{4.18}$$

where $\operatorname{erf}(\cdot)$ is the error function [13] and u is defined in (4.16c).

As can be easily shown, the simplification $w_x = w_y = w$ of the Eq.(4.8) leads to a known calculation of the geometrical attenuation (4.19) of a circular Gaussian beam.

$$\alpha_{\text{geom,circ}} = 1 - \exp\left[-2 \frac{r_{\text{RXA}}^2}{w^2(z)}\right]. \tag{4.19}$$

4.3 Misalignment loss

The previous section describes the geometrical loss in terms of the change of the received optical power P_r as a function of the link distance (range) z. This section introduces and analyses two possible misalignment scenarios and their influence on the link performance; the (lateral) displacement Δ between the relative position of TXA and RXA (shown in Fig.4.2) in the lateral direction and the angular deviation (tilt; pointing error) γ_t of TXA relative to RXA (cf. Fig.4.3). The main cause giving rise to the attenuation due to misalignment is non-uniform intensity distribution of the Gaussian beam. In case of a uniform beam distribution (e.g. using so-called "Top-Hat" beam), the received optical power would not change unless the misalignment is larger than beam dimensions. Other considered causes are the finite divergence θ of the transmitted beam and finite FOV. In the first approximation it would seem that the relation between lateral misalignment Δ and tilt γ_t of TXA depending on the distance z is simply given by

$$\Delta = z \cdot \tan(\gamma_\text{t}). \tag{4.20}$$

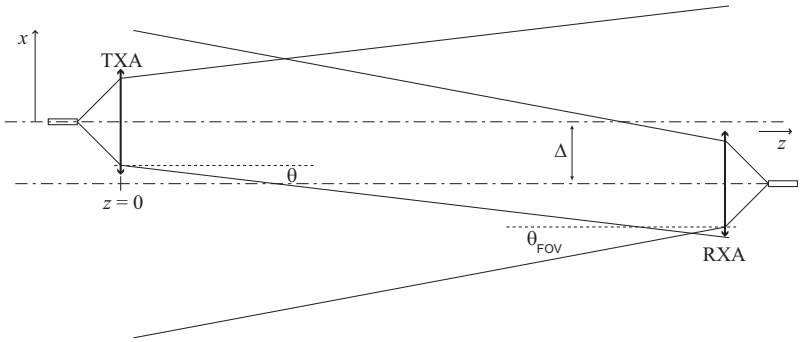

Fig. 4.2: To the explanation of lateral misalignment loss. Δ represents the lateral misalignment and θ and θ_{FOV} stand for the divergence of the transmitter and field-of-view of the receiver, respectively.

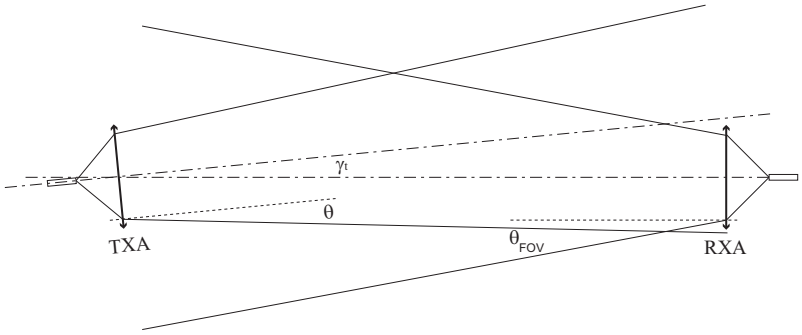

Fig. 4.3: To the explanation of angular misalignment attenuation loss. γ_{t} represents the angular misalignment of the transmitter and θ and θ_{FOV} stand for the divergence of the transmitter and FOV of the receiver, respectively.

The derivation itself is based on the integration of the optical intensity distribution over RXA. Mathematically this situation is expressed in Cartesian coordinates as

$$P_{\mathrm{r}} = \iint_{\Sigma_{\mathrm{RXA}}} I(x, y, z) \mathrm{d}\Sigma_{\mathrm{RXA}}, \tag{4.21}$$

where $I(x, y, z)$ represents the optical intensity distribution of the Gaussian beam in the receiver plane Σ_{RXA}.

First, let's assume only the case of circularly symmetrical beam, when only one (axial) parameter Δ is sufficient to fully describe the lateral misalignment of the two terminals. In order to calculate integral in Eq. (4.21), we must define the integration limits

$$x \in < -r_{\mathrm{RXA}}, r_{\mathrm{RXA}} > \tag{4.22a}$$

$$y \in < \Delta - \sqrt{r_{\mathrm{RXA}}^2 - x^2}, \Delta + \sqrt{r_{\mathrm{RXA}}^2 - x^2} > . \tag{4.22b}$$

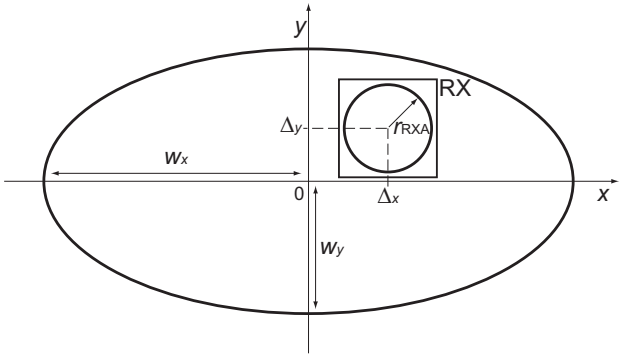

Fig. 4.4: Front view of the misaligned elliptical beam in the receiver plane Σ_{RXA}. Δ_x and Δ_y are displacements and w_y are the beam-widths in x and y axis, respectively, and r_{RXA} is the aperture radius of the receiver RX.

However, in case of elliptically symmetrical beams the situation is more complex. One needs to distinguish between lateral displacement Δ_x and Δ_y in the x and y axis, respectively. For the integration, the optimal choice of integration limits in (4.21) is essential. Proposed integration limits are based on Fig.4.4

$$x \in < \Delta_x - r_{\mathrm{RXA}}, \Delta_x + r_{\mathrm{RXA}} > \tag{4.23a}$$

$$y \in < \Delta_y - \sqrt{r_{\mathrm{RXA}}^2 - x^2}, \Delta_y + \sqrt{r_{\mathrm{RXA}}^2 - x^2} > . \tag{4.23b}$$

Using integration limits in Eq. (4.23) in Eq. (4.21) yields

$$P_{\mathrm{r}}\left(\Delta_x, \Delta_y, z\right) = I(0,0,z) \int_{\Delta_x - r_{\mathrm{RXA}}}^{\Delta_x + r_{\mathrm{RXA}}} \exp\left[\frac{-2x^2}{w_x^2(z)}\right] \int_{\Delta_y - \sqrt{r_{\mathrm{RXA}}^2 - x^2}}^{\Delta_y + \sqrt{r_{\mathrm{RXA}}^2 - x^2}} \exp\left[\frac{-2y^2}{w_y^2(z)}\right] \mathrm{d}y \; \mathrm{d}x. \tag{4.24}$$

Finally, we may write for the lateral misalignment attenuation $\alpha_{\mathrm{mis,ellip}}$ considering the elliptical Gaussian beam

$$\alpha_{\mathrm{mis,ellip}}(\Delta_x, \Delta_y, z) = \sqrt{\frac{2}{\pi w_x^2(z)}} \cdot \int_{\Delta_x - r_{\mathrm{RXA}}}^{\Delta_x + r_{\mathrm{RXA}}}$$

$$\exp\left[\frac{-2x^2}{w_x^2(z)}\right] \left\{ \mathrm{erf}\left[\frac{\sqrt{2}}{w_y(z)}\left(\Delta_y + \sqrt{r_{\mathrm{RXA}}^2 - x^2}\right)\right] - \mathrm{erf}\left[\frac{\sqrt{2}}{w_y(z)}\left(\Delta_y - \sqrt{r_{\mathrm{RXA}}^2 - x^2}\right)\right] \right\} \mathrm{d}x. \tag{4.25}$$

5 ALL-OPTICAL FSO TRANSCEIVER

This chapter follows previous two analytical chapters and describes the development of the fully photonic transceiver. Fully photonic (or all-optical) transceiver stands for a design with no optoelectronic (O/E) and electro-optic (E/O) conversion, i.e. the input optical signal from the optical fiber (OF) is collimated and transmitted to the free-space by means of transmitter optics and on the other side is focused and coupled back into the OF. This approach eliminates distortion and delays introduced by the E/O and O/E conversions needed to transmit electrical signals by optical means; especially in applications, which are already based on the optical signals (e.g. fibre telecommunications), but also in applications, which use coherent properties of the optical beam to transmit time (or synchronisation pulses).

The following chapter shows the synthesis of the transmitter optics design for dual-wavelength all-optical single-aperture (DAS) FSO transmitter followed by the synthesis of the all-optical receiver for OWC.

5.1 Dual-core fibre-based DAS

DC OF consists of two individual fibres (SM800-5.6-125 for 850 nm and SM980-5.8-125 for 1550 nm), cores and claddings of which are stripped down at the output side and molded together into a single jacket. They are used nowadays in many applications, e.g. sensing and gain flattening and their performance has been studied. In the transmitter part of the proposed DAS terminal, similar concept was adopted in order to virtually merge both optical beams. Custom-made DC OF was manufactured for this purpose. The cross-section of the DC OF is shown in Fig.5.1. Cores of the OFs are separated by only 125 μm distance, which allows us to use a single FC/APC connector at the output of the system, which is then collimated by a single lens to the free-space. This approach increases reliability of the whole system by reducing several degrees of freedom compared to the situation with two individual transmitters. If cores are aligned properly in the jacket, both beams propagate in the same physical channel. Also, due to stable position of the cores inside the final fibre, there is no need for alignment of the relative pointing of the beams. The complete schematics of the DAS FSO transmitter is shown in Fig.5.2. On the left-hand side, there are two external FC/APC inputs used when signals are coupled from an external source, e.g. when the terminal is used as an FSO bridge for existing fibre-based network, or when transmitting LDs are located outside the terminal (when controlled conditions are required). The terminal is equipped also with two internal pigtailed LDs, which are via OI connected in each branch (850 and 1550) to the SM fibre coupler, which merges optical signal generated from the

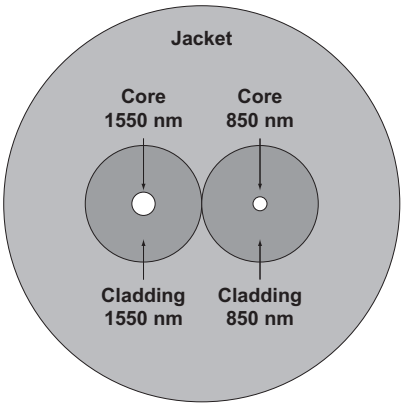

Fig. 5.1: Cross-section of the dual core OF. Distance between centre of the cores is 125µm. Not to scale.

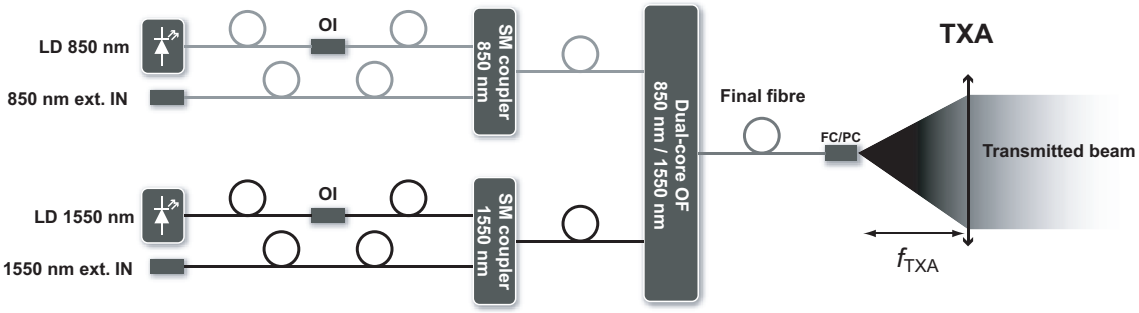

Fig. 5.2: Schematics of the dual-wavelength all-optical single-aperture (DAS) FSO transmitter. Two external inputs and two internal laser diodes (LD) with optical isolator (OI) are in each branch of SM fibre couplet connected to the respective input of a dual-core (DC) final fibre. Output optical beam emerging from the output of the final fibre is coupled to the free-space by the plano-convex lens (TXA) with focal length f_{TXA}. Light gray colour indicates SM OF SM800-5.6-125 for 850 nm, black colour indicates SM OF SM980-5.8-125 for 1550 nm and dark gray colour represents the DC OF. Unless otherwise stated, all optical connectors are FC/APC type.

internal source with the signal coupled via external input to the respective input of the custom-made DC final fibre.

The optomechanical assembly (OMA) of the transmitting optical system should allow change of the relative distance between the final fibre output connector and the collimating lens in order to change the beam divergence angle θ. Moreover,

it should allow for the beam steering and positioning in order to point the beam towards the receiver as precisely as possible. Again, the larger the beam spot at the receiver side, the lower is turbulence-induced power fluctuation, but also the lower is the received optical power. For long-range FSO links, the transmitted power must be increased. The proposed fibre-based FSO terminal has yet another advantage in the possibility of using the erbium-doped fibre amplifier (EDFA), which can increase the output optical power by up to 30 dB [5].

5.2 All-optical receiver: optomechanical design

Optomechanical part of the receiver serves for focusing the received optical beam to the active area of the photosensitive detector or, in our case, for coupling into OF. The critical system requirements include radius r_{RXA} of the receiver aperture (RXA), half-angle θ_{FOV} of field of view (FOV), operating wavelength λ, effective focal length (EFL), f-number f# of the receiving lens, core diameter and acceptance angle of the fibre and others [5]. This section presents considerations and requirements on the OMA RX design used for optical beam coupling from free-space to a SM OF at $\lambda = 1550$ nm.

Final all-optical RX OMA design consists of two main parts; Cassegrain (or Schmidt-Cassegrain) telescope in focal mode used to collect as much beam optical power from the free-space and GRIN lens for its coupling into SM OF. In order to collimate convergent beam at the output of the telescope for the GRIN lens, an aspherical lens can be used. Cassegrain telescope with aspherical lens form a Keplerian telescope. The schematics of the proposed OMA RX is shown in Fig. 5.3.

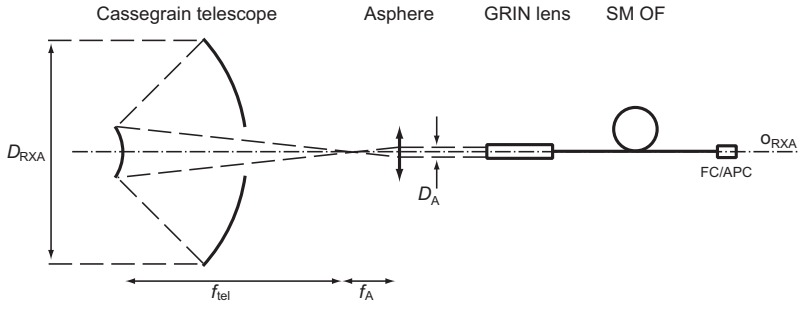

Fig. 5.3: Schematics of the proposed OMA RX design. D_{RXA} and D_{A} stand for the Keplerian telescope diameter and the beam diameter at the output of the asphere, respectively, f_{tel} and f_{A} stand for the telescope and collimating asphere diameter, respectively, o_{RXA} represents the OMA optical axis. Not to scale.

The length l_{KT} of a Keplerian telescope is

$$l_{\mathrm{KT}} = f_{\mathrm{tel}} + f_{\mathrm{A}}, \tag{5.1}$$

where f_{tel} and f_{A} are focal lengths of the telescope and asphere, respectively. The angular magnification M_{a} of the Keplerian telescope, defined as the negative ratio of the focal length f_{tel} to f_{A}, is essential for the estimation of the beam diameter D_{A} at its output, which should not exceed size of the active area of the GRIN lens D_{GRIN}. The beam diameter D_{A} is

$$D_{\mathrm{A}} = f_{\mathrm{A}} \frac{D_{\mathrm{RXA}}}{f_{\mathrm{tel}}}, \tag{5.2}$$

which will be derived later together with M_{a}.

In order to meet the requirement $D_{\mathrm{A}} \leq D_{\mathrm{GRIN}}$, the focal length f_{A} of the asphere must fulfill requirement

$$f_{\mathrm{A}} \leq D_{\mathrm{GRIN}} \frac{f_{\mathrm{tel}}}{D_{\mathrm{RXA}}}. \tag{5.3}$$

Assuming commercially available Cassegrain telescope with $f_{\mathrm{tel}} = 1250$ mm and $D_{\mathrm{RXA}} = 125$ mm

$$f_{\mathrm{A}} \leq 0.5 \frac{1250}{125} = 5 \text{ mm}, \tag{5.4}$$

which narrows the selection down to aspheres with focal length $f_{\mathrm{A}} = 4.50$ mm, which are commercially available (e.g. Thorlabs 355230-C or Newport 5722-H-C), typically with numerical aperture NA ≈ 0.5. In that case the beam diameter at the input of the GRIN lens is

$$D_{\mathrm{A}} = f_{\mathrm{A}} \frac{D_{\mathrm{RXA}}}{f_{\mathrm{tel}}} = 4.51 \frac{125}{1250} = 0.451 \text{ mm} \leq D_{\mathrm{GRIN}}, \tag{5.5}$$

which satisfies the requirement in Eq. (5.3).

There is an alternative to the asphere as coupling element using a bi-concave lens to form a Galileian telescope, instead of the Keplerian type. However, there is no affordable and commercially available bi-concave lens meeting the focal length restriction discussed above.

5.3 OMA alignment tolerances

Relatively small diameter of the optical fibre core poses strict requirements on the alignment tolerances of the whole system. The alignment tolerance of a single lens is proportional to the tolerable focal spot displacement in the perpendicular plane (OF core radius r_{OF} in this case) and inversely proportional to its focal length f. The angular magnification of the optical system gives rise to multiplication of the

Telescope	
Type	Schmidt-Cassegrain
Diameter D_{RXA}	125 mm
Focal length f_{tel}	1250 mm
Primary mirror f-number f#	f/2
Secondary mirror f-number f#	f/20
Telescope f-number f#	f/10
Collimating lens	
Type	Aspheric lens
Model	Thorlabs 355230-C
Focal length f_{A}	4.51 mm
Numerical aperture NA	0.55
Fibre-coupling element	
Type	GRIN lens (SM pigtailed)
Model	50-1550A-APC
Active area diameter D_{GRIN}	0.5 mm
Central wavelength	1550 nm
Beam diameter	0.5 mm
Beam divergence $\mathrm{FOV}_{\mathrm{GRIN}}$	0.25°
Insertion loss	<0.1 dB

Tab. 5.1: Specifications of the all-optical RX design.

angular misalignment at the input of the optical system, which for the proposed system can be written in terms of matrix optics as (cf. Fig. 5.4)

$$\begin{bmatrix} r_{\mathrm{o}} \\ \theta_{\mathrm{o}} \end{bmatrix} = M_4 \cdot M_3 \cdot M_2 \cdot M_1 \begin{bmatrix} r_i \\ \theta_i \end{bmatrix} = \begin{bmatrix} 1 & d_4 \\ 0 & 1 \end{bmatrix} \cdot \begin{bmatrix} 1 & 0 \\ -\frac{1}{f_{\mathrm{A}}} & 1 \end{bmatrix} \cdot \begin{bmatrix} 1 & l_{\mathrm{KT}} \\ 0 & 1 \end{bmatrix} \cdot \begin{bmatrix} 1 & 0 \\ -\frac{1}{f_{\mathrm{tel}}} & 1 \end{bmatrix} \cdot \begin{bmatrix} r_{\mathrm{i}} \\ \theta_{\mathrm{i}} \end{bmatrix}, \quad (5.6)$$

where r_{i} and θ_{i} represent the ray lateral and angular displacement, respectively, in the plane of the telescope input, r_{o} and θ_{o} represent the ray lateral and angular displacement, respectively, in the plane of the GRIN input aperture. M_i stand for the matrices of the individual subsystems of the receiver (cf. Fig. 5.4); telescope modelled as a convex lens M_1, space between telescope and asphere M_2, aspheric lens M_3 and space between asphere and GRIN lens M_4; $l_{\mathrm{KT}} = f_{\mathrm{tel}} + f_{\mathrm{A}}$ represents the distance between telescope and asphere and d_4 represents the distance between asphere and GRIN lens. Multiplying the matrices yields

$$\begin{bmatrix} r_{\mathrm{o}} \\ \theta_{\mathrm{o}} \end{bmatrix} = \begin{bmatrix} d_4 \left(\frac{f_{\mathrm{A}} + f_{\mathrm{tel}}}{f_{\mathrm{A}} f_{\mathrm{tel}}} - \frac{1}{f_{\mathrm{A}}} - \frac{1}{f_{\mathrm{tel}}} \right) - \frac{f_{\mathrm{A}}}{f_{\mathrm{tel}}} & \frac{f_{\mathrm{tel}}}{f_{\mathrm{A}}} d_4 + f_{\mathrm{A}} + f_{\mathrm{tel}} \\ 0 & -\frac{f_{\mathrm{tel}}}{f_{\mathrm{A}}} \end{bmatrix} \begin{bmatrix} r_{\mathrm{i}} \\ \theta_{\mathrm{i}} \end{bmatrix}. \quad (5.7)$$

Fig. 5.4: Schematic representation of the angular alignment tolerance α_{tol} of the proposed receiver. r_{i} and θ_{i} represent the ray lateral and angular displacement, respectively, in the plane of the telescope input, r_{o} and θ_{o} represent the ray lateral and angular displacement, respectively, in the plane of the GRIN input aperture, M_1, M_2, M_3 and M_4 represent matrices of the telescope, space between telescope and asphere, aspheric lens and space between asphere and GRIN lens. Not to scale.

From here, the alignment tolerance estimation yields

$$r_{\mathrm{o}} = \left(\frac{f_{\mathrm{tel}}}{f_{\mathrm{A}}} d_4 + f_{\mathrm{A}} + f_{\mathrm{tel}} \right) \theta_{\mathrm{i}}. \tag{5.8}$$

Let's assume that r_{o} should not exceed the radius of the input aperture of GRIN r_{G} and that $\theta_{\mathrm{i}} = \alpha_{\mathrm{tol}}$. Then, the angular ray misalignment at the RXA is

$$\alpha_{\mathrm{tol}} < \frac{r_{\mathrm{G}}}{M_{\mathrm{A}} d_4 + f_{\mathrm{A}} + f_{\mathrm{tel}}}, \tag{5.9}$$

which after substitution of the parameters from Table 5.1 yields

$$\alpha_{\mathrm{tol}} < \frac{5.10^{-4}}{277.10^{-2} + 4.51.10^{-3} + 1.25} = 0.12 \text{ mrad} = 0.007^{\circ}, \tag{5.10}$$

which is smaller than the used divergence by one order of magnitude. The estimation in (5.9) directly determines the half-angle of receiver's FOV θ_{FOV}.

Now, using Eq. (5.7), will be shown the derivation of expression for angular magnification M_{a} defined after (5.1) and the expression (5.2) for beam size at the input of GRIN lens D_{A}. The angular magnification M_{a} can be derived from Eq. (5.7) for zero displacement r_{o} and r_{i} as

$$\theta_{\mathrm{o}} = -\frac{f_{\mathrm{tel}}}{f_{\mathrm{A}}} \theta_{\mathrm{i}}, \tag{5.11}$$

from which the angular magnification M_{a} is

$$M_{\mathrm{a}} = \frac{\theta_{\mathrm{o}}}{\theta_{\mathrm{i}}} = -\frac{f_{\mathrm{tel}}}{f_{\mathrm{A}}}, \tag{5.12}$$

which for negative f_{A} (concave lens) yields magnification of the Galileian telescope (upright image), whereas for positive f_{A} (convex lens) yields magnification of the Keplerian telescope (inverted image).

Similarly, for beam size D_{A} Eq. (5.7) yields for zero angular displacement θ_{o} and θ_{i}

$$r_{\mathrm{o}} = \left[d_4 \left(\frac{f_{\mathrm{A}} + f_{\mathrm{tel}}}{f_{\mathrm{A}} f_{\mathrm{tel}}} - \frac{1}{f_{\mathrm{A}}} - \frac{1}{f_{\mathrm{tel}}} \right) - \frac{f_{\mathrm{A}}}{f_{\mathrm{tel}}} \right] r_{\mathrm{i}}, \tag{5.13}$$

from which I derived, assuming $r_{\mathrm{o}} = D_{\mathrm{A}}$ and $r_{\mathrm{i}} = D_{\mathrm{RXA}}$, for the beam size at the input of GRIN lens

$$D_{\mathrm{A}} = \left[d_4 \left(\frac{f_{\mathrm{A}} + f_{\mathrm{tel}}}{f_{\mathrm{A}} f_{\mathrm{tel}}} - \frac{1}{f_{\mathrm{A}}} - \frac{1}{f_{\mathrm{tel}}} \right) - \frac{f_{\mathrm{A}}}{f_{\mathrm{tel}}} \right] D_{\mathrm{RXA}}, \tag{5.14}$$

from which the D_{A} can be calculated using parameters in Table 5.1

$$\begin{aligned} D_{\mathrm{A}} &= \left[10^{-2} \left(\frac{4.51.10^{-3} + 1.25}{4.51.10^{-3} \cdot 1.25} - \frac{1}{4.51.10^{-3}} - \frac{1}{1.25} \right) - \frac{4.51.10^{-3}}{1.25} \right] 0.125 = \\ &= 4.51.10^{-4} \text{ m} = 0.451 \text{ mm}, \end{aligned} \tag{5.15}$$

which is in agreement with the result of Eq.(5.2).

In order to verify this estimation, one can benefit from using a computer SW (e.g. ZEMAX).

Due to low FOV of the proposed RX OMA and its tolerance to alignment derived in (5.9) the system, even when ideally aligned, might suffer from critical power fluctuations due to wavefront disturbance causing change in the angle of arrival (AoA) of the optical wave [17]. This angular change of the wavefront incident angle relative to the optical axis is in the order of tens of microradians [18]. In order to compensate for the wavefront disturbance due to turbulence effects, adaptive optics techniques can be used,

5.4 Non-standard atmospheric effects

Not only turbulence is responsible for the AoA fluctuation, but also building and terminal sway. Since there is no general link location, one cannot generalise the influence of the wind on the specific building or terminal stand. It is recommended, however, to take into account this effect prior to the OAM design in order to optimise 1) long-term statistics of the wind speed and direction at the given location, 2) terminal's shape and size, 3) required terminal reliability and link availability and 4) robustness of the terminal stand. The optimisation process is schematically depicted in Fig. 5.5, where tight relation between all of these four parameters is shown.

In terms of wind-induced fading, the aerodynamics of the terminal design is essential. Not only are the curved (rounded) shapes preferred from the rectangular, but also the all-optical transceivers concept allows for more compact terminal design. The all-optical transceiver may be divided into an internal unit with all electronics (laser current drivers) and optics, leaving only the final fibres for signal transmission and reception together with the OMA in the external unit. This approach leaves all the necessary electronics and optical components (lasers, photodiodes) in a more or less stabilised and controlled conditions. Although to change the link direction is not

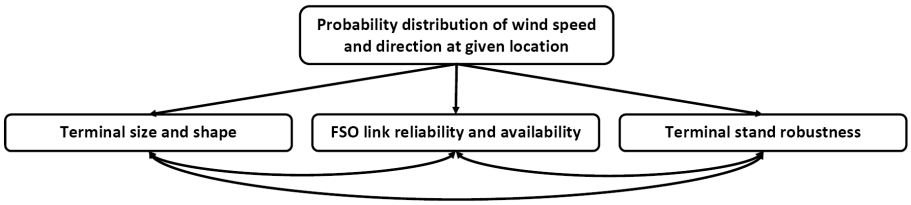

Fig. 5.5: Wind-related FSO link availability estimation model.

always feasible, it is optimal to turn it along the direction of the highest probability of the wind direction according to the long-term measurements.

The influence of the solar radiation on the measured attenuation data as well as the influence of other effects can be studied using duplex testing FSO links. Such links can be also used to study the phenomenon of cross-sensitivity of the measurement of atmospheric influence on various effects and on their homogeneity along the propagation path. Duplex measurement requires each of the terminals to be equipped with both the transmitter and the receiver and hence introduces a redundancy to the measurement. Comparison of the measured data from both directions would effectively reveal inhomogeneity along the path, whether its inhomogeneity of a meteorological event (rain, fog) or misalignment of one of terminals. In case of data mismatch, these data would be excluded from further analysis as faulty.

Last, bot not least significant, effect observed during development of FSO receiver is the inhomogeneous dependency of the sensitivity of photodiode's active area. This effect gives rise to unstable output current reading from PD when the received beam is focused not ideally in its centre, but rather close to the edge of PD. An advantage of the proposed RX design is that it allows to connect a pigtailed PD to its output, where the relative position of the OF and PD is fixed and optimised, what eliminates the dependency of the output current of the PD on the beam position on its active area.

6 CONCLUSION

Fraunhofer diffraction effects (far-field diffraction) have been well described mainly in terms of the beam broadening effect in FSO links. One of the most influential wave effect in OWC nowadays is the Fresnel diffraction, which is also one of the main focuses of the dissertation. Fresnel effects are well known in structural analysis of materials, however, the dissertation sets them into a new aspect of FSO links, where it hasn't been thoroughly studied so far. The thesis then defines the divergent elliptical Gaussian beam as an appropriate approximation of a real laser beam used in FSO systems nowadays. This beam is used as an input function for Fresnel

diffraction integral, which for the first time, introduces and defines Fresnel diffraction integral of a divergent elliptical Gaussian beam restricted by a circular aperture. The expression is in form of Fourier transform and in Cartesian coordinates, which offers straightforward computer simulations of the near-field diffraction effects.

The diffraction integral has been derived also in terms of Bessel function integration model. Although this model assumes circularly symmetrical scenario, it allowed for a definition of the diffraction pattern contrast, which was used to estimate the influence of the Fresnel diffraction on the performance of the FSO link. An optimal ratio between link distance, wavelength and transmitter aperture size was identified in order to minimise the diffraction pattern contrast and the systems's misalignment sensitivity associated with it.

Restriction of the beam gives rise not only to the aforementioned wave effects, but also to optical power attenuation, which was analysed by means of electromagnetic optics. The dissertation introduced four independent derivations of the geometrical attenuation calculations assuming elliptically symmetrical Gaussian beam on a circular receiver aperture. It also provided analysis of the impact of various misalignment scenarios on the link reliability and availability. The analysis is useful during the link design phase when the proper attenuation and misalignment analysis is crucial for link budget estimation.

Development of the receiver optomechanical assembly was more challenging due to the requirement on the receiver aperture size and limitation of the overall length. The design incorporates the Cassegrain telescope and the aspherical lens to form a Keplerian telescope. It produces a relatively small collimated beam, which is then focused into a single-mode fibre using the fibre-pigtailed GRIN lens. I presented the performance analysis by means of the geometric (matrix) optics to derive and optimise the relevant receiver parameters. The alignment tolerance showed that despite relatively low FOV, the receiver is capable of dealing with turbulence-induced change of the beam angle of arrival.

BIBLIOGRAPHY

[1] K.-D. LANGER and J. GRUBOR, "Recent developments in optical wireless communications using infrared and visible light," in *Transparent Optical Networks, 2007. ICTON '07. 9th International Conference on*, vol. 3, pp. 146–151, 2007.

[2] E. LEITGEB, T. PLANK, P. PEZZEI, D. KRAUS, and J. POLIAK, "Integration of fso in local area networks – combination of optical wireless with wlan and

dvb-t for last mile internet connections," in *Proceedings of 2014 19th European Conference on Networks and Optical Communications*, pp. 120–125, 2014.

[3] H. HENNIGER and O. WILFERT, "An introduction to free-space optical communications," *Radioengineering*, vol. 19, no. 2, pp. 203–212, 2010.

[4] A. K. MAJUMDAR and J. C. RICKLIN, *Free-Space Laser Communications: Principles and Advances*. Springer, 2008.

[5] H. HEMMATI, A. BISWAS, and I. DJORDJEVIC, "Deep-space optical communications: Future perspectives and applications," *Proceedings of the IEEE*, vol. 99, no. 11, pp. 2020–2039, 2011.

[6] L. C. ANDREWS, *Laser Beam Propagation through Random Media*. SPIE Press, 2005.

[7] G. PARCA, "Optical wireless transmission at 1.6-tbit/s (16x100 gbit/s) for next-generation convergent urban infrastructures," *Optical Engineering*, vol. 52, p. 116102, Nov. 2013.

[8] D. BOROSON, J. SCOZZAFAVA, D. MURPHY, B. ROBINSON, and H. SHAW, "The lunar laser communications demonstration (llcd)," in *Space Mission Challenges for Information Technology, 2009. SMC-IT 2009. Third IEEE International Conference on*, pp. 23–28, July 2009.

[9] O. WILFERT, Z. KOLKA, V. BIOLKOVA, P. KRIVAK, L. DORDOVA, O. FISER, and J. NEMECEK, "Dual optical wireless test link," in *Proc. SPIE 7091, Free-Space Laser Communications VIII*, vol. 7091, pp. 70910W–70910W–8, 2008.

[10] Z. GHASSEMLOOY, W. POPOOLA, and S. RAJBHANDARI, *Optical wireless communications; system and channel modelling with MATLAB*. CRC Press, 2012.

[11] J. ALDA, "Laser and gaussian beam propagation and transformation," *Encyclopedia of Optical Engineering*, pp. 999–1013, 2003.

[12] E. a. HOVENAC, "Fresnel diffraction by spherical obstacles," *American Journal of Physics*, vol. 57, no. 1, pp. 79 – 84, 1989.

[13] I. S. GRADSHTEYN and I. M. RYZHIK, *Table of integrals, series, and products*. Elsevier/Academic Press, Amsterdam, seventh ed., 2007. Translated from the Russian, Translation edited and with a preface by Alan Jeffrey and Daniel Zwillinger, With one CD-ROM (Windows, Macintosh and UNIX).

[14] J. POLIAK, J. KOMRSKA, and O. WILFERT, "Restricted beam analysis for fso links," in *Antennas and Propagation (EUCAP), 2012 6th European Conference on*, pp. 335–339, 2012.

[15] G. D. GILLEN and S. GUHA, "Modeling and propagation of near-field diffraction patterns: A more complete approach," *American Journal of Physics*, vol. 72, no. 9, p. 1195, 2004.

[16] J. POLIAK, P. PEZZEI, P. BARCIK, E. LEITGEB, L. HUDCOVA, and O. WILFERT, "On the derivation of exact analytical fso link attenuation model," *Transactions on Emerging Telecommunications Technologies*, vol. 25, no. 6, pp. 609–617, 2014.

[17] H. T. EYYBOGLU and Y. K. BAYKAL, "Effects of laser multimode content on the angle-of-arrival fluctuations in free-space optical access systems," in *Proc. SPIE 5473, Noise in Communication*, vol. 5473, pp. 184–190, 2004.

[18] H. T. EYYBOGLU and Y. BAYKAL, "Angle-of-arrival fluctuations for general-type beams," *Optical Engineering*, vol. 46, no. 9, pp. 096001–096001–8, 2007.

Ing. Juraj Poliak

Contact Information

Technicka 12
Brno CZ-61600
Czech Republic
tel: +420 54114 6558
fax: +420 54114 6597
mailto: xpolia00@stud.feec.vutbr.cz
web: http://www.urel.feec.vutbr.cz/OptaBro/

Oponice 190
Oponice SK-95614
Slovak Republic
mobile: +420 608 202 918
mobile: +421 948 666 165
poliak.juraj@gmail.com

Citizenship Slovak Republic

Research Interests Free-space optical communications modelling, optical wave effects – diffraction modelling, study of various optical environments in which the laser beam propagates, fully photonic FSO terminals and non-standard atmospheric phenomena.

Education

Brno University of Technology, Brno, Czech Republic

09/2011 – 09/2014 (exp.) PhD. Candidate, Electronics and Communication

- Thesis Topic: *Diffraction effects in the transmitted laser beam*
- Supervisor: Prof. Otakar Wilfert

09/2009 – 06/2011 Master of Engineering (Dipl-Ing.), Electronics and Communication

- Thesis Topic: *Effect of optical elements on transmitted laser beam*
- Supervisor: Prof. Otakar Wilfert
- With results of the thesis author won 2^{nd} prize on EEICT 2011
- Author was awarded the Dean price in 2011
- The thesis was acknowledged by the Lambert publishing house

09/2005 – 06/2009 Bachelor of Engineering (Bc.), Electronics and Communication

- Thesis Topic: *Synchronnous detection of modulated optical signals*
- Supervisor: Dr. Petr Drexler

Masaryk University, Brno, Czech Republic

09/2007 – 06/2010 Bachelor of Physics (Bc.), Applied Physics – Astrophysics

- Thesis Topic: *Detection of Radioastronomical Sources*
- Supervisor: Dr. Filip Hroch
- The thesis was acknowledged by the Lambert publishing house

Academic Appointments

PhD. Candidate since 09/2011

Department of Radio Electronics, Brno University of Technology

- since 08/2011 member of OptaBro – the Optical Communications Research Group
- since 06/2012 research assistant at CEITEC – Central European Institute of Technology
- since 01/2013 PhD. student employee at SIX – Sensor, Information and Communication Systems Centre
- experience with national, international, European and ESA project proposals
- active member of COST Action IC1101 Opticwise

Teaching Assistant

- Quantum and Laser Electronics (winter semester 2011)
- Optical Communication Fundamentals and Optoelectronics (summer semester 2013)
- Computer and Communication Networks (summer semester 2013)

Research Stays

Graz University of Technology, Austria 01/2012 – 03/2012

- Supervisor Prof. Erich Leitgeb, leader of the Research Group for Optical Communications (OptiKom), Institute of Microwave and Photonics Engineering
- Development of general analytical (elliptical) Gaussian beam free-space attenuation model for FSO links considering various misalignments
- Passed exams in Optical Communications (in German) with "'Excellence"'

Pforzheim University of Applied Sciences, Germany 10/2012 – 12/2012

- Supervisor: Prof. Friedemann Mohr, leader of the Electrooptics and Measurement & Instrumentation Lab, Dept. of Information Technology
- Derivation of the mathematical model of the Y-branch laser tuning characteristics for use in sensor applications

Professional Experience

FEI, Czech republic, Brno, Czech Republic

02/2010 to 10/2011 *Intern for Technical Support Group*

- Quality-related data mining supporting design changes on electron microscopes
- Processing of proposals and requirements (SW, HW, electronics) on new products

Motorola, Brno, Czech Republic

06/2007 to 09/2007 *Service technician*

- Service of barcode readers
- Quality inspection of wireless modules for various products

Computer Skills

Programming languages Matlab (advanced user), MathCAD (advanced user), VBA (certified advanced user), Python, C/C++

Office tools Proficient LaTeX and Microsoft Office (Word, Excel, Outlook, Powerpoint) user, Certified advanced user of Excel 2007 (Certificate of advanced methods and functions in Microsoft Excel 2007)

Specialized SW Zemax, PSpice, Eagle, Origin Pro

Language Skills

Slovak native speaker

Czech advanced

English advanced (ESOL CAE-C1 level passed, 78 %)

Italian upper-intermediate

German intermediate

Spanish basic knowledge of the language

Miscellaneous

Driving license category A1, B (pursuing B+E); 100k+ km driving experience

Personal qualities

Hard-working, team player, flexible, self-motivated.

Hobbies

Music, Physics, Travelling, Flying.

ABSTRACT

The thesis was set out to investigate on the wave and electromagnetic effects occurring during the restriction of an elliptical Gaussian beam by a circular aperture. First, from the Huygens-Fresnel principle, two models of the Fresnel diffraction were derived. These models provided means for defining contrast of the diffraction pattern that can be used to quantitatively assess the influence of the diffraction effects on the optical link performance. Second, by means of the electromagnetic optics theory, four expressions (two exact and two approximate) of the geometrical attenuation were derived. The study shows also the misalignment analysis for three cases – lateral displacement and angular misalignment of the transmitter and the receiver, respectively. The expression for the misalignment attenuation of the elliptical Gaussian beam in FSO links was also derived. All the aforementioned models were also experimentally proven in laboratory conditions in order to eliminate other influences. Finally, the thesis discussed and demonstrated the design of the all-optical transceiver. First, the design of the optical transmitter was shown followed by the development of the receiver optomechanical assembly. By means of the geometric and the matrix optics, relevant receiver parameters were calculated and alignment tolerances were estimated.

KEYWORDS

Free-space optical link, Fresnel diffraction, geometrical loss, pointing error, all-optical transceiver design

ABSTRAKT

Dizertačná práca pojednáva o vlnových a elektromagnetických javoch, ku ktorým dochádza pri zatienení eliptického Gausovského zväzku kruhovou apretúrou. Najprv boli z Huygensovho-Fresnelovho princípu odvodené dva modely Fresnelovej difrakcie. Tieto modely poskytli nástroj pre zavedenie kontrastu difrakčného obrazca ako veličiny, ktorá kvantifikuje vplyv difrakčných javov na prevádzkové parametre optického spoja. Následne, pomocou nástrojov elektromagnetickej teórie svetla, boli odvodené štyri výrazy (dva presné a dva aproximatívne) popisujúce geometrický útlm optického spoja. Zároveň boli skúmané tri rôzne prípady odsmerovania zväzku - priečne posunutie a uhlové odsmerovanie vysielača, resp. prijímača. Bol odvodený výraz, ktorý tieto prípady kvantifikuje ako útlm elipticky symetrického Gausovského zväzku. Všetky vyššie uvedené modely boli overené v laboratórnych podmienkach, aby sa vylúčil vplyv iných javov. Nakoniec práca pojednáva o návrhu plne fotonického optického terminálu. Najprv bol ukázaný návrh optického vysielača nasledovaný vývojom optomechanickej sústavy prijímača. Pomocou nástrojov geometrickej a maticovej optiky boli vypočítané parametre spoja a odhad tolerancie pri zamierení spoja.

KLÍČOVÁ SLOVA

Optický bezdrôtový spoj, Fresnelova difrakcia, geometrický útlm, chyba zamierením, návrh plne optického spoja.